Transition from resistive ballooning to η_i driven turbulence in tokamaks

A. Zeiler[a] and D. Biskamp
Max-Planck-Institut für Plasmaphysik, EURATOM Association, 85748 Garching, Germany

J. F. Drake and B. N. Rogers
Institute for Plasma Research, University of Maryland, College Park, Maryland 20742

(Received 4 November 1997; accepted 13 April 1998)

The mechanisms of turbulent transport in the collisional tokamak edge plasma are investigated linearly and nonlinearly, focusing specifically on the transition from resistive modes to ion temperature gradient driven (η_i) modes. Linear eigenvalue calculations demonstrate that resistive ballooning and toroidal η_i modes can exist as separate roots with similar growth rates but with differing structure along the magnetic field. While the typical transverse scale length of the resistive modes depends strongly on collisionality, the transverse scales of the η_i mode are essentially independent of the collisionality, even in the absence of any assumption on the adiabaticity of the electrons. Three-dimensional nonlinear simulations quantitatively describe the transition between the resistivity dominated outermost edge and regions with moderately higher temperature where resistive modes are stabilized and the collisionless η_i mode dominates. A significant result is that the η_i modes continue to drive significant particle transport even in regimes where the linear stability analysis indicates the electrons are dominantly adiabatic. The particle transport is driven by the nonadiabatic, long-parallel-wavelength component of the wave spectrum. As in earlier calculations of η_i turbulence, the self-generated poloidal flows are relatively strong, much stronger than in cold ion simulations, and strongly influence the saturation levels and associated transport rates. The implications of the results for understanding edge transport and density and temperature profiles are discussed. © *1998 American Institute of Physics.* [S1070-664X(98)03007-9]

I. INTRODUCTION

The quantitative prediction of turbulent transport remains one of the most challenging problems in theoretical plasma physics, as well as in the design of future toroidal confinement experiments. Whereas the ion energy confinement in the hot plasma core seems to be largely controlled by collisionless ion temperature gradient modes,[1,2] resistive modes drive the turbulence in the more collisional edge and the ion temperature dynamics is usually completely ignored in this regime.[3,4] In simulations of η_i mode turbulence, on the other hand, resistivity is usually ignored[1,2,5–8] and only the nonadiabatic electron dynamics associated with mirror-trapped electrons are retained.[9] The particular importance of the plasma edge was recently highlighted by a critical temperature gradient model in which the core temperature was found to be proportional to the temperature at the plasma edge.[10] For a successful prediction of the global confinement it is therefore of crucial importance to investigate the transition between these two distinct physical regimes and to study the impact of the ion temperature gradient on the dynamics of collisional edge plasma.

In this paper we show that the ion temperature gradient contributes to the transport at the plasma edge in two different ways: as an additional drive contributing to the resistive ballooning instability and as an independent instability (the η_i mode), which remains insensitive to the collisionality despite the finite electrical conductivity. In general, the edge fluctuations make a transition from resistive ballooning driven turbulence, to nonlinear-driven, resistive turbulence,[4,11–13] and finally to η_i driven turbulence in moving from the scrape-off layer towards the plasma core. This transition arises from the dramatic changes in both the conductivity and the gradient scale lengths across the edge. Since the resistive ballooning modes and the toroidal η_i modes have comparable growth rates [of order $c_s/(L_pR)^{1/2}$, where R is the major radius and L_p is the pressure scale length] the relative strength of the turbulence associated with each drive is linked to the characteristic scale lengths of the fluctuations transverse to B. In the tokamak edge region the transverse scale of the toroidal η_i mode, in particular, is very sensitive to the ratio of the density scale length L_n to the major radius R through the parameter $\epsilon_n = 2L_n/R$ in a way which differs substantially from the more extensively studied core: the very small value of ϵ_n in the extreme edge forces the η_i generated turbulence to remain at scale lengths comparable to the ion Larmor radius ρ_i. With increasing values of ϵ_n, further inside the plasma column, the η_i turbulence extends to longer wavelength and becomes a stronger driver of transport. The strength of the resistive ballooning mode has the opposite dependence on radius: in the low temperatures characteristic of the extreme edge the transverse scale length of the resistive ballooning turbulence greatly exceeds ρ_i and with increasing temperature the scale length decreases until finally the resistive ballooning mode is completely stabilized by diamagnetic effects.[14] Thus, tokamak edge trans-

[a]Electornic mail: asz@ipp-garching.mpg.de

port is dominated by resistive ballooning modes in the extreme edge and by η_i modes further inside, the location of the transition being determined by other key parameters such as η_i and the collisionality.

As seen previously in η_i simulations,[1,15] we find that self-generated poloidal flows can play an important role in saturating the fluctuations and controlling the rate of transport. In particular, the poloidal flows become very strong when the ion diamagnetic velocities are comparable to typical velocities of the turbulent eddies. In a separate publication we show that the poloidal flows arise from the Kelvin-Helmholtz instability of radial flows driven by resistive ballooning or η_i modes. These poloidal flows do not, however, cause complete stabilization of the turbulence since they are themselves unstable and break up. Thus, they must be considered a part of the turbulence.

In the regime where the η_i driven turbulence dominates, the particle transport remains surprisingly large, of the order of 30% of the ion energy transport, even in regimes in which the linearly unstable modes are nominally adiabatic. This transport is driven by the long parallel wavelength component of the wave spectrum.

II. BASIC EQUATIONS

Our investigations are based on the electrostatic drift-Braginskii equations[16] in a flux-tube domain using field-aligned coordinates,[3,4] which we write here in dimensionless form:

$$\nabla_\perp \cdot \frac{d}{dt}\nabla_\perp(\phi+\tau\alpha_d p_i)+\hat{C}\frac{p_e+\tau p_i}{1+\tau}+\frac{\partial^2 h}{\partial z^2}=0, \tag{1}$$

$$\frac{dn}{dt}+\frac{\partial\phi}{\partial y} -\left[\epsilon_n\hat{C}(\phi-\alpha_d p_e)-\epsilon_v\frac{\partial v_\parallel}{\partial z}-\alpha_d\epsilon_n(1+\tau)\frac{\partial^2 h}{\partial z^2}\right]=0, \tag{2}$$

$$\frac{dT_e}{dt}+\eta_e\frac{\partial\phi}{\partial y}-\frac{2}{3}\left[\epsilon_n\hat{C}\left(\phi-\alpha_d p_e-\frac{5}{2}\alpha_d T_e\right) -\epsilon_v\frac{\partial v_\parallel}{\partial z}-1.71\alpha_d\epsilon_n(1+\tau)\frac{\partial^2 h}{\partial z^2}+\kappa_\parallel\frac{\partial^2 T_e}{\partial z^2}\right]=0, \tag{3}$$

$$\frac{dT_i}{dt}+\eta_i\frac{\partial\phi}{\partial y}-\frac{2}{3}\left[\epsilon_n\hat{C}\left(\phi-\alpha_d p_e+\frac{5}{2}\tau\alpha_d T_i\right) -\epsilon_v\frac{\partial v_\parallel}{\partial z}-\alpha_d\epsilon_n(1+\tau)\frac{\partial^2 h}{\partial z^2}\right]=0, \tag{4}$$

$$\frac{dv_\parallel}{dt}+\epsilon_v\frac{\partial}{\partial z}\frac{p_e+\tau p_i}{1+\tau}=0, \tag{5}$$

with

$$p_e=n+T_e,\quad p_i=n+T_i,\quad h=\phi-\alpha_d(p_e+0.71T_e),$$

$$\nabla_\perp^2=\left[\frac{\partial}{\partial x}+2\pi\hat{s}z\frac{\partial}{\partial y}\right]^2+\frac{\partial^2}{\partial y^2},$$

$$\hat{C}=[\cos(2\pi z)+2\pi\hat{s}z\sin(2\pi z)-\epsilon]\frac{\partial}{\partial y}+\sin(2\pi z)\frac{\partial}{\partial x},$$

$$\frac{d}{dt}=\frac{\partial}{\partial t}-\left(\frac{\partial\phi}{\partial y}\frac{\partial}{\partial x}-\frac{\partial\phi}{\partial x}\frac{\partial}{\partial y}\right).$$

The time and space units,

$$t_0=\left(\frac{RL_n}{2}\right)^{1/2}\frac{1}{c_s},\quad L_z=2\pi q_a R,$$

$$L_\perp=2\pi q_a\left(\frac{\nu_{ei}R\rho_s}{2\Omega_{ce}}\right)^{1/2}\left(\frac{2R}{L_n}\right)^{1/4}, \tag{6}$$

are chosen to balance the three terms in Eq. (1) and are the natural choices for the resistive ballooning mode[3] (but not for the η_i mode which is essentially independent of the collisionality). This normalization yields the dimensionless parameters

$$\alpha_d=\frac{\rho_s c_s t_0}{(1+\tau)L_n L_\perp},\quad \epsilon_n=\frac{2L_n}{R},\quad \epsilon_v=\frac{c_s t_0}{L_z}, \tag{7}$$

$$\tau=\frac{T_{i0}}{T_{e0}},\quad \kappa_\parallel=1.6\alpha_d^2\epsilon_n(1+\tau),\quad \eta_e=\frac{L_n}{L_{T_e}},$$

$$\eta_i=\frac{L_n}{L_{T_i}}, \tag{8}$$

with $c_s^2=(T_{e0}+T_{i0})/m_i$, $\rho_s=c_s/\Omega_{ci}$, $\hat{s}$ the magnetic shear parameter, $\epsilon=a/R$, the profile e-folding lengths L_n, L_{T_e}, and L_{T_i}, and where we have assumed that the ions are singly charged. The ratio between the transverse scale lengths $L_\perp$ and ρ_s is important for understanding the relation between resistive ballooning and η_i mode turbulence. In our dimensionless units this ratio can be expressed as

$$\rho_s/L_\perp=(1+\tau)\alpha_d\epsilon_n^{1/2}. \tag{9}$$

The electron and ion diamagnetic (ω_*), curvature (ω_c) drift frequencies, and parallel electron diffusion rate $D_{\parallel e}$ play an important role in the evaluation of the linear growth rates of both resistive ballooning and the η_i modes. For reference we write these first in dimensional,

$$\omega_{*e}=\frac{k_y c T_e}{eBL_n},\quad \omega_{*i}=\frac{k_y c T_i}{eBL_n}(1+\eta_i),$$

$$\omega_{ce}=\frac{2k_y c T_e}{eBR}(\cos(z/qR)+\hat{s}(z/qR)\sin(z/qR)-\epsilon),$$

$$D_{\parallel e}=2T_e/m_e\nu_{ei},$$

and then dimensionless units,

$$\omega_{*e}=k_y\alpha_d,\quad \omega_{*i}=k_y\alpha_d\tau(1+\eta_i),$$

$$\omega_{ce}=k_y\alpha_d\epsilon_n(\cos(2\pi z)+\hat{s}(2\pi z)\sin(2\pi z)-\epsilon),$$

$$D_{\parallel e}=(1+\tau)\epsilon_n\alpha_d^2, \tag{10}$$

where in both cases $\omega_{ci}=\omega_{ce}\tau$. The treatment of the ion temperature dynamics in these equations differs from that in most previous fluid treatments of η_i driven turbulence.[5–7] The major difference is that in the ion temperature equation,

Eq. (4), the compressibility terms arising from the polarization and ion curvature drifts are fully retained. The role of the polarization drift can be seen more explicitly if the $\partial^2 h/\partial z^2$ term is replaced using Eq. (1). At scale lengths comparable to ρ_s these terms are important and can not be neglected. The retention of these terms prohibits the separation of the ion diamagnetic and **E×B** drifts in Eq. (1) for the vorticity (see Ref. 16 for details). The linear theory of the slab η_i mode using these equations in the adiabatic limit yields growth rates that are in much better agreement with kinetic treatments than earlier fluid models.[8]

Though in contrast to most previous treatments the equations properly retain all finite Larmor radius corrections contained in the Braginskii equations, we emphasize that perturbations with wavelengths comparable to the ion gyroradius are not accurately described. For the parameters characteristic of the plasma edge, however, the turbulence arising from our model is dominated by perturbations with transverse scales much larger than the ion Larmor radius. The inaccurate description of the very short wavelength disturbances, therefore, probably does not significantly impact the transport. The Braginskii model also does not account for collisionless effects such as trapped particle dynamics. Therefore the equations are appropriate to describe the collisional edge and the adjacent region of a somewhat higher temperature where the collisionality is sufficient to prevent particle trapping, i.e., for ν_{*e}, $\nu_{*i} > 1$ with

$$\nu_{*e} = \nu_{ei} qR/\epsilon^{3/2} v_{te},$$

with a similar expression for ν_{*i}. For the Axisymmetric Divertor Experiment (ASDEX-U), for example, the values of typical local parameters at the location of the middle of the edge pedestal in the low confinement mode (L-mode) just prior to the low-to-high (L–H) transition are $T_e = 100$ eV, $T_i = 120$ eV, $n = 3.0 \times 10^{13}/\mathrm{cm}^3$ with $q = 4$, $R = 165$ cm, and $a = 50$ cm[17] which yields $\nu_{*e} = 22$ and comparable ν_{*i}. The parameters for DIII-D[18] are similar, while the Alcator C-MOD[19] has a substantially higher collisionality. The Braginskii equations are therefore a reasonable model for studying the edge and the dynamics of the L–H transition in these machines since typical collisionalities preclude the dynamics of trapped particles from influencing the system. As a final caveat, we note that the equations also do not accurately describe the dissipation in toroidal geometry. This requires the addition of magnetic pumping[20] as well as ion parallel thermal conduction. This additional physics is required to accurately model transport, since the strength of the self-generated poloidal flows, which is controlled by this damping, can influence the overall level of the turbulence. This subject will be addressed more fully in a follow-up paper.

III. LINEAR STABILITY

Before proceeding with a presentation of the results of nonlinear simulations using Eqs. (1)–(5), we discuss the linear instability properties of the equations with an emphasis on exploring the relationship between resistive ballooning and curvature driven η_i modes. In this discussion we neglect the electron temperature fluctuations ($T_e = 0$), since their contribution to both resistive ballooning modes and the η_i mode is inhibited by parallel heat conduction.[21]

The basic relationship between η_i and resistive ballooning modes can be understood from a simplified set of the linearized equations in which the ambient density gradient and the parallel velocity $v_\parallel$ are neglected. The coupled equations for ϕ, n, and p_i (normalized, respectively, to T_{e0}/e, n_0, and $n_0 T_{e0}$) are

$$-k_\perp^2 \rho_{se}^2 \gamma(\phi + p_i) + i\omega_{ce} p_i + D_{\parallel e} \frac{\partial^2}{\partial z^2}(\phi - n) = 0, \tag{11}$$

$$\gamma n + D_{\parallel e} \frac{\partial^2}{\partial z^2}(\phi - n) = 0, \tag{12}$$

$$\gamma p_i + i\omega_{*i}\phi = 0, \tag{13}$$

where for clarity we have written the independent parameters in dimensional units where γ is the growth rate of the mode and the subscript e indicates that the quantity is to be evaluated with the electron temperature. The relationship between resistive ballooning and toroidal η_i modes can most easily be seen by examining a local dispersion relation with $\partial/\partial z = ik_\parallel$,

$$k_\perp^2 \rho_{se}^2 (\gamma - i\omega_{*i}) - \frac{\omega_{ce}\omega_{*i}}{\gamma} + \frac{\gamma k_\parallel^2 D_{\parallel e}}{\gamma + k_\parallel^2 D_{\parallel e}} = 0. \tag{14}$$

For a given set of equilibrium parameters relevant to the plasma edge, both the resistive ballooning mode and the η_i mode can exist simultaneously with comparable values of $k_\perp$ but with different values of $k_\parallel$. The resistive ballooning mode typically has a parallel scale length of the order of the parallel connection length πqR[3,14] and the last term in Eq. (14) can be neglected. We then obtain the resistive ballooning dispersion relation,[14]

$$\gamma(\gamma - i\omega_{*i}) = \frac{\omega_{ce}\omega_{*i}}{k_\perp^2 \rho_{se}^2}, \tag{15}$$

which in this simple limit is the same as that of the ideal ballooning mode. In the plasma edge the η_i mode is much more localized along the magnetic field line with the localization being determined by the sound wave. The result is that $\gamma \ll k_\parallel^2 D_{\parallel e}$ and Eq. (14) reduces to the dispersion relation of the toroidal η_i mode,

$$(1 + k_\perp^2 \rho_{se}^2)\gamma^2 - i\omega_{*i} k_\perp^2 \rho_{se}^2 \gamma - \omega_{ce}\omega_{*i} = 0. \tag{16}$$

The modes are unstable as long as $k_\perp \rho_{se}$ is not too large. Since the ambient density gradient has been discarded, there is no η_i threshold for instability in Eq. (16). Thus, the resistive ballooning and toroidal η_i modes are simply limiting cases of a more general dispersion relation. The drive terms for both modes are the same, as are the dynamics of the ions. Only the electron dynamics differ, the electrons being adiabatic in the case of the η_i mode. The growth rates of the two modes peak at around the same level, of the order of the ideal ballooning growth rate $c_s/(L_p R)^{1/2}$. An important difference, however, is that the growth rates peak at different scale lengths. In the case of the resistive ballooning mode the

growth rate peaks at the scale length $L_\perp$ defined in Eq. (6), which depends on the plasma collisionality. The maximum growth rate of the η_i mode on the other hand occurs for $k_\perp \rho_s \lesssim 1$. These different scale lengths will play an important role in understanding the results of the nonlinear simulations.

The linear stability of the η_i mode based on Eqs. (1)–(5) differs substantially from earlier fluid treatments[5–7] because of the retention of the polarization and curvature drifts in the ion temperature equation. We, therefore, briefly review the adiabatic limit of these equations where analytic solutions of the equations can be readily obtained. This limit corresponds to $\partial^2/\partial z^2$ large so that $h \sim 0$ or $\phi = \alpha_d n$. The $\partial^2 h/\partial z^2$ terms are eliminated by subtracting Eqs. (1) and (2) and Eqs. (2) and (4) with the appropriate multipliers. The resulting equations plus the equation for the parallel velocity can be combined into a single second order equation for the total pressure $p = n + \tau p_i$,

$$c_{se}^2 \frac{\partial^2 p}{\partial z^2} + \gamma(i\omega_{ce} - \gamma k_\perp^2 \rho_{se}^2) p - \frac{\gamma(\gamma + i\omega_{*e})\left(\gamma - \frac{5}{3} i\omega_{ce}\tau\right)}{\gamma\left(1 + \frac{5}{3}\tau\right) - i\omega_{*e}\tau\left(\eta_i - \frac{2}{3}\right) - \frac{5}{3} i\omega_{ce}\tau(1+\tau)} \times p = 0. \tag{17}$$

We have again written the equation in dimensional units, since the normalization of the equations based on the resistive ballooning scaling laws does not simplify the η_i mode equations, which are independent of the resistivity. The second and third terms in brackets yield the local dispersion relation for the instability,

$$\gamma^2\left(1 + \left(1 + \frac{5}{3}\tau\right) k_\perp^2 \rho_{se}^2\right) + i\gamma\left[\omega_{*e} - \omega_{ce}\left(1 + \frac{10}{3}\tau\right) - k_\perp^2 \rho_{se}^2\left(\omega_{*e}\tau\left(\eta_i - \frac{2}{3}\right) + \frac{5}{3}\omega_{ce}\tau(1+\tau)\right)\right] - \omega_{ce}\left(\omega_{*e}\tau\left(\eta_i - \frac{7}{3}\right) + \frac{5}{3}\omega_{ce}\tau(1+\tau)\right) = 0. \tag{18}$$

This dispersion equation retains only the curvature drive since the sound wave, which is essential for the slab η_i mode, has been discarded. The third term, proportional to the local curvature ω_{ce}, is the drive for the instability, and is destabilizing for

$$\eta_i > \frac{7}{3} - \frac{5}{3}(1+\tau)\frac{\omega_{ce}}{\omega_{*e}}. \tag{19}$$

That this term being positive is a sufficient condition for instability can be seen by examining the cross term (proportional to γ) in Eq. (18). If the condition, Eq. (19), is satisfied the term proportional to γ is zero for a suitable choice of $k_\perp \rho_{se}$ so that instability is always possible over some range of $k_\perp$. On the other hand, since $\omega_{ce}/\omega_{*e} \sim \epsilon_n \ll 1$ in the edge region, the unstable modes are at a rather short wavelength,

$$k_y^2 \rho_i^2 \sim \frac{1}{\eta_i - \frac{2}{3}}, \tag{20}$$

unless η_i is well above threshold. It should also be emphasized that the Braginskii equations are not valid for $k_\perp \rho_i > 1$, so care must be taken that the modes that dominate the spectrum of turbulence in the nonlinear simulations have a sufficiently long wavelength. For more moderate values of ϵ_n, long wavelength modes can be unstable even when η_i is of moderate size. The condition for the instability of long wavelength modes is

$$4\omega_{ce}\left(\omega_{*e}\tau\left(\eta_i - \frac{7}{3}\right) + \frac{5}{3}\omega_{ce}\tau(1+\tau)\right) > \left(\omega_{*e} - \omega_{ce}\left(1 + \frac{10}{3}\tau\right)\right)^2. \tag{21}$$

This is an important condition, since it is typically the longest wavelength component of the unstable spectrum that dominates the transport (see the discussion at the end of this section). This equation can be rewritten in a simpler dimensionless form as a threshold in η_i,

$$\eta_i > \frac{7}{3} - \frac{5}{3}\epsilon_n \overline{\omega}_c (1+\tau) + \frac{1}{4\tau\epsilon_n \overline{\omega}_c} \times \left(1 - \left(1 + \frac{10}{3}\tau\right)\epsilon_n \overline{\omega}_c\right)^2, \tag{22}$$

with $\overline{\omega}_c = \cos(2\pi z) + \hat{s} 2\pi z \sin(2\pi z) - \epsilon \sim 1$ depending on the spatial localization of the mode (discussed below). For the tokamak edge where ϵ_n is small, the quadratic term on the right side of the equation is a rapidly decreasing function of ϵ_n so that the long wavelength instability condition effectively becomes a condition on ϵ_n, i.e., Eq. (22) is satisfied for sufficiently large ϵ_n. We note that a similar long wavelength limit was derived in Ref. 22.

It is well known that the sound wave can localize core η_i modes in local regions of bad curvature[23] and the localization is even stronger in the plasma edge. The localization of the long wavelength modes arises from the variation of the curvature ω_{ce} with z, which can trap the modes. For $\hat{s} > 0.5$ the curvature has a minimum at $z = 0$ and peaks at a location z_0 given by the transcendental equation $\tan(z_0/qR) = [\hat{s}/(1 - \hat{s})] z_0/qR$. For $\hat{s} = 1.0$, $z_0 = 0.25$, corresponding to a poloidal angle of $\pi/2$. Expansion of Eq. (17) around either of these locations yields the standard Weber equation, which can be solved for bounded eigenmodes and the associated eigenvalues. The eigenvalue of the lowest order mode is given by the local dispersion relation in Eq. (18) evaluated either at $z = 0$ or at z_0, the correction due to nonlocality being small. The width Δ of the lowest order mode in both cases is given by

$$\frac{\Delta}{qR} \sim \left(\frac{1}{k_y \rho_s q}\right)^{1/2} \left(\frac{L_p}{R}\right)^{1/8}. \tag{23}$$

The modes remain localized for wave vectors down to

$$k_\perp \rho_s \sim \frac{1}{q}\left(\frac{L_p}{R}\right)^{1/4}. \tag{24}$$

In the edge the pressure scale length is of order 2 cm with $q\sim 3$ so for $R\sim 180$ cm, the modes remain localized down to $k_\perp \rho_s \sim 0.1$. There are also typically a substantial number of higher harmonics with growth rates comparable to the lowest order mode. This is again a consequence of the short pressure scale length in the edge region which effectively weakens the tendency of sound waves to disperse the modes parallel to the magnetic field. Thus, above threshold a rather broad spectrum of long wavelength modes can have a strong ballooning character in the plasma edge.

We now present the results of a more complete analysis of the linear stability of Eqs. (1)–(5). We again neglect electron temperature fluctuations T_e but include the parallel ion dynamics. Only modes with $k_x = 0$ are retained. This corresponds to solutions with no radial variation on the outside of the torus at $z=0$ (see Ref. 4 for a detailed description of the field-aligned flux-tube coordinates). The eigenvalue calculations are performed in the range of typical plasma edge parameters $\alpha_d \sim 1$, $\epsilon_n \sim 0.05$, $\eta_i \sim 1$, $\hat{s}=1$, and $\epsilon_v \sim 0.005$. Note that the shorter scale lengths in the edge cause ϵ_n and ϵ_v to have much smaller values than in the plasma core. The numerical results support the discussion of the simple dispersion relation in Eq. (14) and the solution of the η_i equation in Eq. (17). First, the resistive ballooning and the curvature driven η_i mode can appear as distinct roots at comparable $k_\perp$ but with significantly different scale lengths along the magnetic field. Second, the η_i mode has multiple roots whose growth rates are essentially independent of the plasma resistivity. Third, the ion pressure gradient strongly enhances the resistive ballooning mode.

In Fig. 1 we show the growth rate γ versus k_y for various parameters. The lower solid curve in Fig. 1(a) is the resistive ballooning mode root for $\eta_i = 0.5$, which is the only unstable mode for these parameters. The upper solid and dashed curves in Fig. 1(a) illustrate the spectrum of unstable modes for $\eta_i = 3$. For this value of η_i there are a large number of roots with comparable growth rates. At high k these are toroidal η_i modes localized around $z=0$. In the limit $\epsilon_v = 0$ the growth rates reduce to the local solution of the dispersion relation in Eq. (18). The peak in the solid curve at long wavelength corresponds to the resistive ballooning mode, with a growth rate which is enhanced by the increase in η_i. It is significantly less adiabatic than the other roots in Fig. 1(a). The resistive ballooning mode appears as distinct root only for $k_\perp L < 1.5$ and then crosses over to an η_i root at higher values of $k_\perp$. We were unable to find a continuation of the resistive ballooning mode above this value of $k_\perp$. An important point to note is that in this parameter regime the resistive ballooning mode and η_i modes can exist simultaneously at long wavelengths. Their spatial variations in the z direction differ substantially. The η_i mode wave functions exhibit rapid oscillations ($\partial/\partial z$ large) which enables the electrons to be adiabatic while the resistive ballooning mode with a weaker z variation retains its nonadiabatic character. This can be seen in Fig. 1(b), which shows the eigenfunctions of the pressure perturbation for the two types of modes.

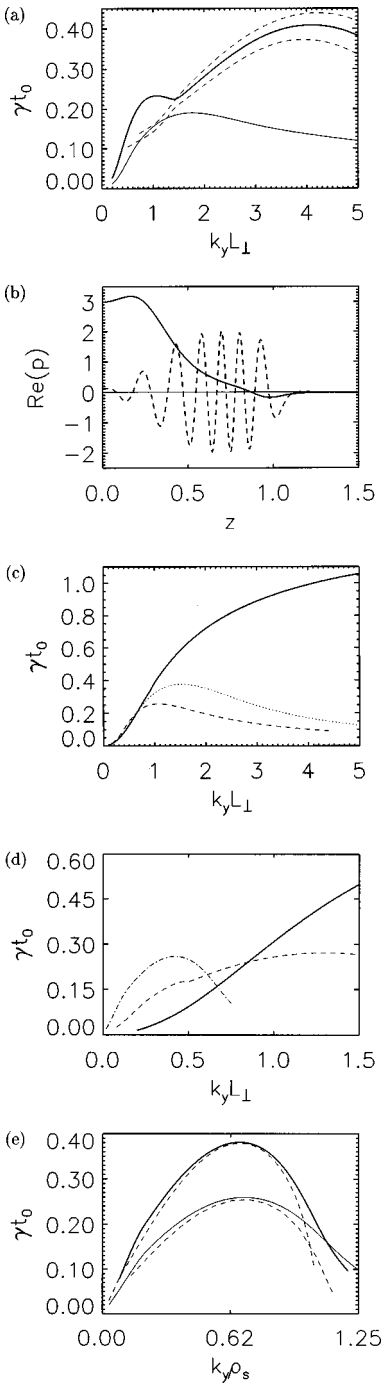

FIG. 1. The linear growth rate γ versus k_y: (a) $\alpha_d = 0.5$, $\epsilon_n = 0.05$, $\epsilon_v = 0.005$, $\eta_i = 0.5$ (lower solid line), $\eta_i = 3$ (upper solid and dashed lines); (b) pressure eigenfunctions corresponding to uppermost solid and dashed lines in (a) at $k_y = 0.7$; (c) $\epsilon_n = 0.01$, $\eta_i = 3$, $\epsilon_v = 0.0$, $\alpha_d = 0$ (solid), $\alpha_d = 0.25$ (dotted), $\alpha_d = 0.5$ (dashed); (d) $\epsilon_n = 0.3$, $\eta_i = 3$, $\epsilon_v = 0.005$, $\alpha_d = 0$ (solid), $\alpha_d = 0.5$ (dashed), and $\alpha_d = 1.5$ (dot-dashed); (e) $\epsilon_n = 0.3$, $\alpha_d = 1.5$, $\epsilon_v = 0.005$, $\eta_i = 5.0$ (upper curves), and $\eta_i = 3.0$ (lower curves).

The solid and dashed curves represent the eigenfunctions corresponding to the uppermost solid and dashed curves in Fig. 1(a) at $k_y = 0.7$. The nonadiabatic component (not shown) of the η_i mode (dashed curve) is over one hundred times smaller than that of the resistive ballooning mode (solid curve).

The behavior of the transition from the resistive balloon-

ing to the η_i mode with increasing diamagnetic parameter α_d depends critically on whether the long wavelength condition for the η_i instability given in Eq. (22) is satisfied. When this condition is not satisfied (for small ϵ_n, τ, and η_i), the resistive ballooning mode spectrum is stabilized by diamagnetic effects. This is shown in Fig. 1(c) where the growth rate of resistive ballooning modes is plotted for several values of α_d with $\epsilon_n=0.01$ and $\eta_i=3.0$ (see also Ref. 14).

On the other hand, when the long wavelength instability threshold for the η_i mode is satisfied and α_d is increased, the growth rate of long wavelength resistive ballooning modes also increases. The modes become increasingly adiabatic and the wavefunctions become spatially localized around $z=0.25$. Eventually, the growth rate converges on the value calculated from the local η_i mode dispersion relation in Eq. (18), independent of the resistivity. In effect, the resistive ballooning mode no longer exists and is replaced by the η_i mode. This transition is shown in Fig. 1(d). The growth rate is shown for $\alpha_d=0.0$ (solid), $\alpha_d=0.5$ (dashed), and $\alpha_d=1.5$ (dot-dashed) with $\epsilon_n=0.3$ and $\eta_i=3.0$.

Finally, the η_i mode regime is illustrated in Fig. 1(e), where we plot the growth rate of the lowest order modes as a function of $k\rho_s$, ρ_s being the more natural scale length of the instability in this limit, for $\eta_i=3{,}5$ with $\alpha_d=1.5$, $\epsilon_n=0.3$ and other parameters as in Fig. 1(a). At each value of η_i two roots are shown. At long wavelength the most unstable root corresponds to an η_i mode localized around $z=0.25$ and the other root to the mode localized around $z=0$ (corresponding to the analytic solutions discussed earlier). The growth rates are accurately given by the local solutions of the dispersion relation in Eq. (18). Thus, the unstable modes are essentially adiabatic and therefore insensitive to the plasma resistivity. At short wavelength both roots are localized around $z=0$ and are again accurately given by the local dispersion relation evaluated at this location, the difference between the two eigenvalues arising because the dashed curve corresponds to a higher order eigenmode. Increasing η_i strongly enhances the growth rate of the instability consistent with Eq. (18).

Since resistive ballooning and η_i mode turbulence can exist simultaneously, an important issue is the relative importance of the two as transport mechanisms. For η_i small only the resistive ballooning mode is unstable. For α_d large the resistive ballooning mode is stabilized by electron and ion diamagnetic effects and based on linear theory the η_i mode must dominate the transport (the relative importance of the nonlinear instability[4,11–13] will be discussed later).

In the regime where both modes are unstable their peak growth rates are comparable [$\gamma\sim 1/t_0\sim c_s/(RL_p)^{1/2}$]. Transport is, however, not necessarily dominated by the mode with the largest growth rate. In the case of the resistive ballooning turbulence, transport is dominated by the longest unstable modes which remain strongly ballooning, i.e., modes with the resistive scale lengths $L_\perp$ in Eq. (6).[3,4] Thus,

$$D_\perp\sim L_\perp^2/t_0\sim(2\pi q)^2\rho_e^2\nu_{ei}\frac{R}{L_p}. \tag{25}$$

The transport from the η_i mode is more complex. When the long wavelength instability criterion in Eq. (22) is not satisfied, the turbulence has a characteristic scale length given by ρ_i [see Eq. (20)]. The simple mixing length estimate $D_\perp\sim\rho_i^2/t_0$ implies that η_i transport will dominate that of resistive ballooning modes when

$$\frac{\rho_s^2}{L_\perp^2}=\epsilon_n\alpha_d^2(1+\tau)^2>1. \tag{26}$$

When the condition in Eq. (22) for the instability of long wavelength modes is satisfied, transport by the η_i mode is dominated by longer scales. A reasonable hypothesis is that, as in the case of resistive ballooning, transport is dominated by the longest wavelength modes which remain strongly ballooning. This ballooning condition is given in Eq. (24). Combining this characteristic scale length with the linear growth rate of long wavelength modes in Eq. (18) yields the transport rate

$$D_\perp\sim\frac{c_s\rho_s^2}{(L_pR)^{1/2}}\left(\frac{q^4R}{L_p}\right)^{1/4}. \tag{27}$$

The first factor in this expression corresponds to the usual scaling for transport based on η_i modes with transverse scales ρ_i and growth rates $c_s/(L_pR)^{1/2}$.[2] The enhancement factor $(q^4R/L_p)^{1/4}$ arises from the shift to long wavelength given in Eq. (24). Again, comparing this diffusion rate with that from resistive ballooning, the transport due to η_i modes will dominate when

$$\frac{\rho_s^2}{L_\perp^2}>\frac{1}{q}\left(\frac{L_p}{R}\right)^{1/4}. \tag{28}$$

This condition is typically satisfied when the long wavelength threshold for η_i modes is also satisfied. In this regime, therefore, transport by η_i driven turbulence will dominate that due to resistive ballooning modes.

IV. RESULTS FROM NONLINEAR SIMULATIONS

We now proceed to study the transition between the various instability regimes with simulations using the complete set of nonlinear Eqs. (1)–(5). Due to the different scale lengths of the turbulence the box size is varied from $16L_\perp\times16L_\perp\times3L_z$ in the nonlinearly driven regime up to $45L_\perp\times45L_\perp\times3L_z$ for some runs in the η_i mode regime. The numerical algorithms, including the viscosities, are described in detail in Refs. 4, 21.

In the low α_d ($\alpha_d\sim0.5$) resistive ballooning regime the ratio $\rho_s/L_\perp$ is always small [see Eq. (9)] for the small values of ϵ_n typical for the plasma edge. For larger values of ϵ_n, however, long wavelength modes are unstable [see Eq. (22)] and the η_i mode can also be important in this regime. With the exception of this special case, the nonlinear simulations confirm that the resistive ballooning mode dominates the transport. The change compared to the cold ion limit[3,4] depends on the relative strength of two competing effects: the additional drive due to η_i versus the stabilization due to the ion diamagnetic drift.

TABLE I. Turbulent transport for $\alpha=1.25$, $\tau=1$, $\eta_i=2.5$, and different values of ϵ_n. Other parameters are $\hat{s}=1$, $\eta_e=1$, $\kappa_\parallel=0.05$, $\epsilon_v=0.005$, and $\epsilon=0.2$. The transport rates are time-averaged and measured on the outside of the torus ($z=0,\pm1$) and on the inside of the torus ($z=\pm0.5$).

		$\langle nv_r\rangle$		$\langle T_iv_r\rangle$		$\langle T_ev_r\rangle$	
ϵ_n	$\rho_s/L_\perp$	Out	In	Out	In	Out	In
0.085	0.73	0.082	0.017	0.57	0.1	0.039	0.021
0.075	0.68	0.066	0.015	0.4	0.07	0.037	0.019
0.06	0.61	0.055	0.015	0.26	0.07	0.036	0.018
0.05	0.56	0.014	0.005	0.06	0.03	0.008	0.007
0.02	0.35	0.013	0.006	0.047	0.024	0.012	0.006
0.01	0.25	0.052	0.035	0.16	0.11	0.07	0.055

In the high-α_d ($\alpha_d>1$) regime, however, the η_i mode can become important for the small ϵ_n typical of the plasma edge. In this regime the resistive ballooning mode is stable and in the absence of ion thermal effects the turbulence is sustained by a nonlinear instability, which is strong when its characteristic scale length, which is typically comparable to $L_\perp$, is greater than ρ_s.[4,11,12,21] For finite ion temperature we show in Table I the transport rates for $\alpha_d=1.25$, $\eta_i=2.5$, and a range of values of ϵ_n, corresponding to a variation of the ratio $\rho_s/L_\perp$ [see Eq. (9)]. For $\epsilon_n=0.085$ ($\rho_s\sim L_\perp$) the ion heat flux is large and dominates the particle and electron thermal flux, demonstrating the adiabatic nature of the underlying turbulence and the dominance of the η_i mode instability. The transport exhibits a large inside/outside asymmetry caused by the ballooning character of the curvature driven mode. For the parameters of this run, the threshold for the instability of long wavelength modes in Eq. (22) is satisfied. Reducing ϵ_n to 0.06 strongly reduces the ion heat flux which is a consequence of the stabilization of long wavelength modes [Eq. (22) is no longer satisfied]. The transport rates decrease further until $\epsilon_n\simeq0.05$. At this point the transition to nonlinearly driven turbulence occurs, with the transport rates steadily increasing with further reductions in ϵ_n. The inside/outside asymmetry is now absent, a characteristic feature of the nonlinear instability, since it is not driven by the unfavorable curvature. The particle and energy diffusion coefficients are of the same order, which is evidence for the nonadiabatic nature of the drive mechanism.

In Fig. 2 we show plots of T_i in the plane perpendicular to the magnetic field at the low and high field sides of the torus. Whereas at low ϵ_n, high α_d (nonlinear instability), no significant difference in the structure of the turbulence is observed between the inside and outside midplane, the high ϵ_n, high-α_d regime (η_i instability) exhibits a strong inside/outside asymmetry. The mode is localized on the outside of the torus, which leads to a twisted structure on the inside due to the high parallel conductivity along the sheared magnetic field. The different scale size of the turbulence is also visible in the fluctuation spectrum of the ion temperature, which we show in Fig. 3 for the nonlinearly driven turbulence ($\epsilon_n=0.01$) and the η_i mode turbulence ($\epsilon_n=0.085$). Note the presence of large amplitude, long wavelength modes with finite k_x, especially in the η_i mode regime. These correspond to poloidal sheared flows ($k_y=0$), which play a significant role in the saturation of the turbulence.[1]

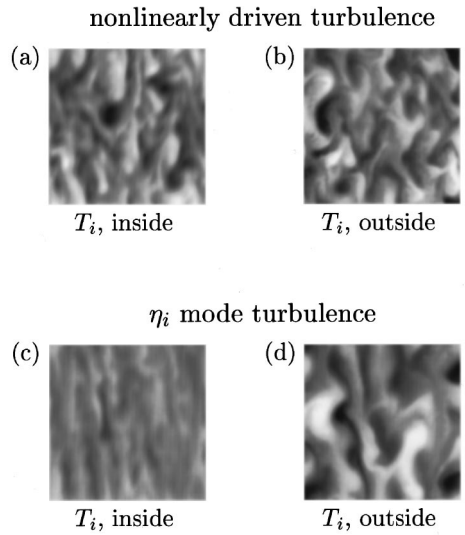

FIG. 2. The structure of T_i at the inside and outside midplane. The plots show poloidal cross-sections (x-y plane) after saturation, the poloidal angle increasing upwards, and the ambient gradients pointing to the left. White indicates high and black low temperature. Plots (a) and (b) were obtained with $\alpha_d=1.25$, $\epsilon_n=0.01$, $\eta_i=2.5$, and the box size $16L_\perp\times16L_\perp\times3L_z$, plots (c) and (d) with $\alpha_d=1.25$, $\epsilon_n=0.075$, $\eta_i=2.5$, and the box size $32L_\perp\times32L_\perp\times3L_z$.

Finally, in Fig. 4 we show the flux-surface averaged ion thermal flux $\Gamma_T=\langle T_iv_x\rangle$ versus time in the η_i regime (corresponding to $\epsilon_n=0.085$ in Table I) and the time averaged flux versus z. The dotted lines indicate the standard deviation due to the time variation of the system. The flux peaks away from $z=0$ as expected from the off-midplane localization of the long wavelength component of the spectrum discussed previously.

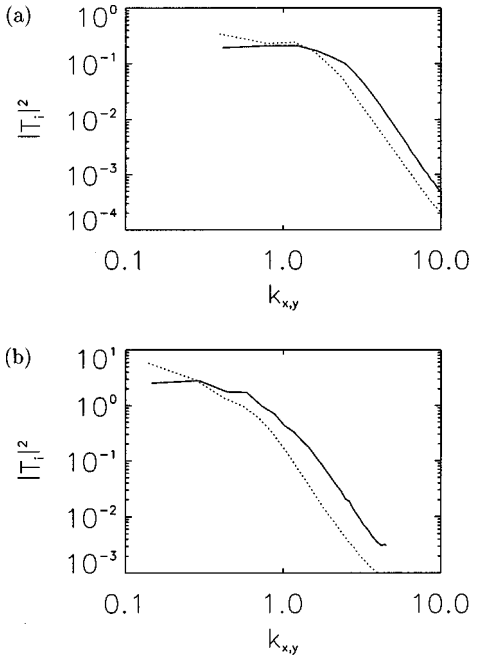

FIG. 3. Time averaged spectra of the ion temperature in k_x (solid) and k_y (dotted) for $\alpha_d=1.25$, $\eta_i=2.5$, and $\epsilon_n=0.01$ (a), $\epsilon_n=0.085$ (b).

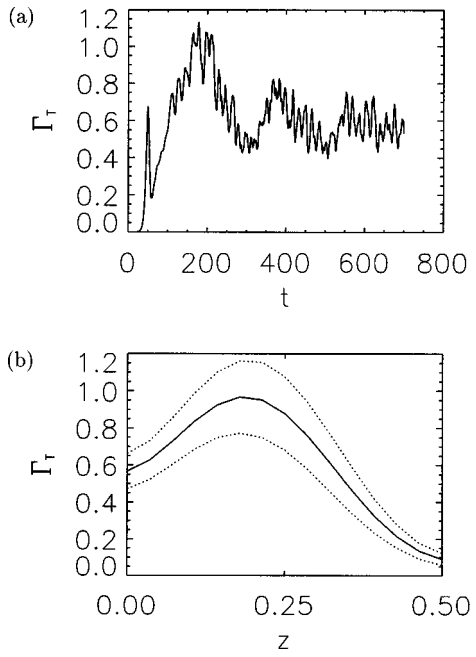

FIG. 4. (a) Flux-surface averaged ion heat flux $\Gamma_T=\langle T_i v_x\rangle$ as a function of time t for $\alpha=1.25$, $\epsilon_n=0.085$, and $\eta_i=2.5$. To obtain the heat flux in dimensional units, Γ_T needs to be multiplied by $(L_\perp^2/t_0)\times(T_{i0}/L_n)$. (b) Time averaged thermal flux versus z for the same run. The time average is taken over the interval $200\leqslant t\leqslant 700$. The outside of the torus is located at $z=0$ and the inside at $z=0.5$. The dotted lines indicate the standard deviation due to the time variation of the system.

Investigations of η_i driven turbulence in the plasma core have been largely carried out in the adiabatic regime where the equations are independent of resistivity or electron Landau dissipation. An important question in the present model is whether the resistivity [specifically the parallel electron diffusion rate as given in Eq. (10)], which enters the equations through the parameter α_d, alters the basic scale lengths of the turbulence. To test this, we have carried out simulations for two different values of α_d (1.25 and 1.75) with all other parameters the same. In Fig. 5 we show the transverse correlation functions of the ion temperature at the outside of the torus for the two different runs. The space scales have been normalized to ρ_s because in our normalization α_d also changes the value of ρ_s, which is a fundamental scale length in η_i driven turbulence. The correlation functions for these two values of α_d have basically the same scale lengths when normalized to the value of ρ_s (which differs by a factor of 1.4 between the two simulations). The underlying turbulence

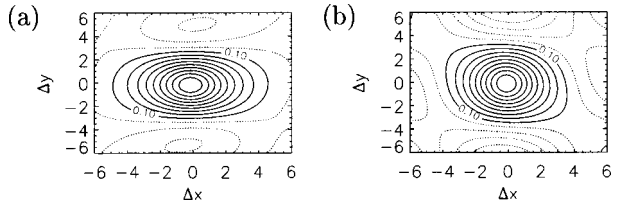

FIG. 5. The correlation function of T_i in the poloidal plane for η_i driven turbulence in the region of bad curvature for (a) $\alpha_d=1.25$, (b) $\alpha_d=1.75$ and all other parameters identical. The space scales are normalized to ρ_s.

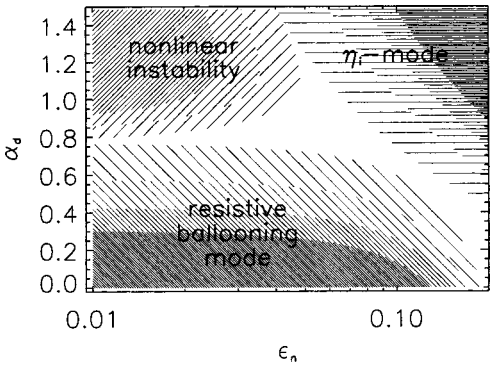

FIG. 6. The parameter space indicating the regions where the various instabilities dominate the turbulence and transport.

in the η_i regime is, therefore, basically insensitive to the parallel electron dissipation.

In previous simulations of η_i driven turbulence,[1] it was found that poloidal sheared flow was self-generated during the growth of the turbulence and played a fundamental role in controlling the rate of the ion energy transport, the transport differing by a factor of 10 with and without the poloidal sheared flow. We have similarly found that the self-generated poloidal flows play an important role in the saturation of the turbulence in regions where the ion diamagnetic drifts are large and specifically in the regime where the η_i mode drives the turbulence. These poloidal flows are generated by a Kelvin-Helmholtz-like instability of the radial flows associated with ballooning instabilities, strongly enhanced by the ion diamagnetic drifts.

The anomalous particle diffusion rate in the η_i mode regime remains surprisingly large, of the order of 20%–30% of the ion energy diffusion rate with a weak variation with the plasma collisionality. The linearly unstable eigenmodes in the η_i regime are dominantly adiabatic, since they are well localized along the magnetic field in the region of bad curvature, as discussed previously in the section on linear stability. Nevertheless, the eigenmodes have a long parallel scale length component. This component of the eigenmode is not adiabatic and is responsible for driving the particle transport. Consistent with this picture, the time dependence of the particle transport tracks the details of the time dependence of the ion energy transport very accurately, as would be expected from the nonadiabatic component of the linear eigenmode.

To more easily visualize the regions where the three primary instabilities dominate, in Fig. 6 we present a diagram of the $\alpha_d-\epsilon_n$ parameter space for $\eta_i\simeq 2.5$. In the region $\alpha_d<0.75$ and ϵ_n small the resistive ballooning mode dominates the transport. For $\alpha_d>1$ but $\epsilon_n\lesssim 0.05$ the nonlinear instability dominates and finally for $\alpha_d>1$ and $\epsilon_n\gtrsim 0.1$ the η_i mode dominates.

V. CONCLUSIONS

In the low β limit being studied in this paper, there are three dominant instabilities which play an important role in the plasma edge region: the resistive ballooning mode, a nonlinear drift-wave instability, and the η_i instability. The

region where each instability dominates depends on the parameters, but the resistive ballooning mode typically dominates in the lowest temperature region, the nonlinear instability dominates at intermediate temperatures, and the η_i mode is important at higher temperatures where the gradient scale lengths are greater. Consistent with previous results,[3,4,14,21] we find that plasma edge turbulence has two distinct scale lengths: a resistive scale length $L_\perp$ defined in Eq. (6) and the conventional gyro scale length ρ_s. The turbulence also has two distinct time scales: the growth time of the ideal ballooning mode $t_0=(L_nR)^{1/2}/c_s$, which characterizes the resistive ballooning and the η_i modes; and a time based on the diamagnetic frequency of the resistive scale length $L_\perp$. The ratio of these two times,

$$\alpha_d=\frac{\rho_s c_s t_0}{(1+\tau)L_n L_\perp}, \tag{29}$$

measures the strength of the diamagnetic drifts in the plasma edge and can also be considered a measure of the edge collisionality. A second important parameter,

$$\epsilon_n=\frac{2L_n}{R}, \tag{30}$$

controls the effective compressibility, including the electron parallel conductivity, the strength of the ion sound waves, and the perpendicular compressibility. An important difference between turbulence in the edge compared to the core is the size of this parameter. It is much smaller in the edge than in the core because the edge pressure scale lengths are only on the order of a few centimeters while in the core they are comparable to the minor radius a. Additional parameters which, in particular, affect the stability of the η_i mode are η_i and the ion to electron temperature ratio τ. For completeness it should be noted that in addition to these parameters the magnetic shear $\hat{s}$ plays a significant role in determining the growth rate of the η_i mode.[24]

Before discussing how these parameters specifically control turbulence in the edge, we show in Fig. 7 two representative profiles of edge density and temperature with the corresponding profiles of η_i, α_d, ϵ_n, and $\rho_s/L_\perp$. The density profiles are tanh-shaped and we choose parameters consistent with those measured in present day tokamaks (see, for example, Refs. 25, 26). The plots are for a deuterium plasma with $T_i/T_e=\tau=1$, $B=2.5$ T, $R=1.65$ m, $q_a=4$, and $Z_{eff}=2.5$. The temperature profiles in the two cases are chosen such that η_i decreases from $\eta_i=2.5$ at the inner edge of the domain towards $\eta_i=1$ at the outermost plasma edge. The density in the second set of plots has been increased by a factor of 3 and the temperatures have been decreased by a factor of 1.5. The parameter α_d increases with increasing temperature and then falls off as the gradients flatten out. The parameter ϵ_n increases from a small value to a relatively large value as the gradients flatten and the corresponding scale lengths increase. For profiles that do not become flatter in the core region, α_d increases monotonically, and ϵ_n increases much less rapidly. The main effect of the increased

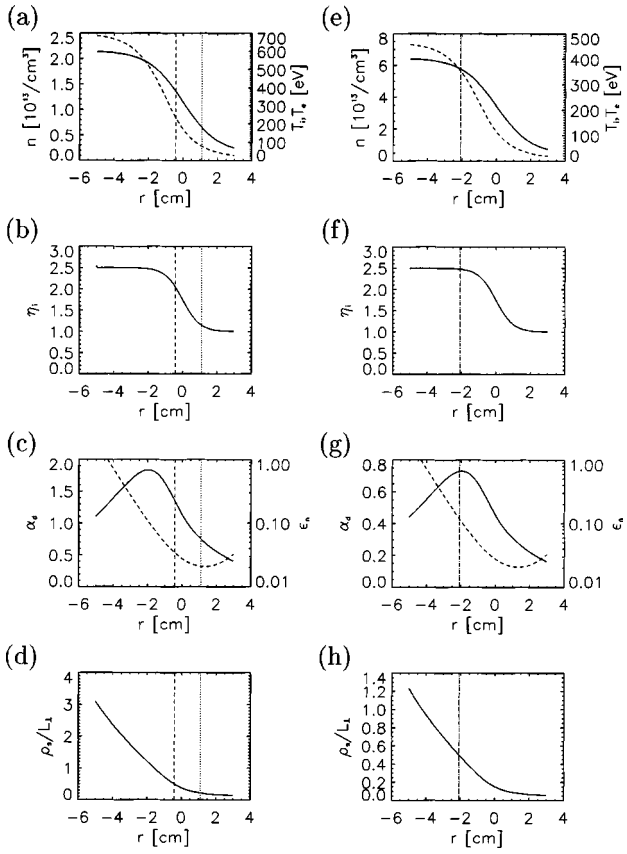

FIG. 7. Parameters and transport in a tanh-shaped profile. The profile of n (solid), and T_e, T_i (dashed) is shown in (a) and (e); the other parameters are $R=165$ cm, $B=2.5$ T, $q_a=4$, $m_i/m_H=2$, $Z_{eff}=2.5$. The resulting values for η_i and α_d (solid) and ϵ_n (dashed) are plotted in Figs. (b), (f) and (c), (g), which yields the ratio $\rho_s/L_\perp$ [Figs. (d), (h)].

density is to reduce α_d, thus reducing the strength of the diamagnetic drifts, and to increase the scale length $L_\perp$ and therefore reduce the ratio $\rho_s/L_\perp$.

Resistive ballooning modes typically remain strong for $\alpha_d<0.75$, depending on the actual values of τ and η_i. The characteristic transverse scale length of the turbulence in this case is several times the resistive scale length $L_\perp$ with the parallel correlation length scaling like πqR. In the case of the low density profile the resistive ballooning mode is limited to a very small region on the outside edge of the plasma. The inner edge of the resistive ballooning region is denoted by a vertical dotted line in the plots in Fig. 7. In the high density case the resistive ballooning turbulence extends much further into the region of high temperature.

Conventional drift waves are stable in plasma with a sheared magnetic field. Nevertheless, turbulence is nonlinearly sustained even in the absence of a linear instability if the parallel electron diffusion rate is not too large[4,11,12] and if the transport from the resistive ballooning modes does not overpower that of the drift waves. The later condition typically requires $\alpha_d>0.75$ while the former requires $\rho_s/L_\perp<0.5$. The turbulence in this case again has a transverse scale length which depends on the resistivity and a parallel correlation length which typically exceeds πqR. In the low density profile in Fig. 7 the nonlinear drift-wave regime lies

between the vertical dotted and dashed lines. The nonlinear drift wave is stabilized by high parallel electron conductivity on the left boundary and is overpowered by the resistive ballooning mode on the right boundary. In the higher density profile where α_d is smaller, there is no region where the nonlinear instability plays a significant role since the resistive ballooning mode is too strong.

The η_i mode can be unstable in the plasma edge. However, it remains rather weak because the characteristic scale lengths of the turbulence are of order ρ_i unless ϵ_n is sufficiently large to destabilize long wavelength perturbations. The threshold condition for long wavelength modes is given in Eq. (22). For $\tau=1$ and $\eta_i=2.5$ this threshold is exceeded for $\epsilon_n \gtrsim 0.07$. Above this threshold the characteristic scale length of the η_i driven turbulence substantially exceeds ρ_s. The characteristic parallel correlation length of the turbulence in this case is also of order $\pi q R$. In the low density case in Fig. 7 the η_i turbulence dominates the transport to the left of the vertical dashed line. The turbulence remains relatively weak until the long wavelength threshold is exceeded. The transport rate then increases dramatically. In the higher density case the η_i mode is again dominant to the left of the vertical dashed line. The transition, however, occurs close to the region where long wavelength disturbances are unstable.

In the low density example in Fig. (7) there is a minimum in the transport rate as a function of radius in the region between the nonlinear drift-wave instability and the η_i mode. This is because the η_i mode is only weakly unstable because long wavelength modes remain stable at small ϵ_n and because ϵ_n and α_d are sufficiently large to weaken the nonlinear instability. This minimum in the transport rate can be seen most clearly in the data shown in Table I, where the transport rate from a sequence of runs is shown with fixed $\alpha_d=1.25$ and varying ϵ_n. The profiles shown in the Fig. 7 are, of course, not consistent with the calculated transport rates. The conclusion to be drawn from this minimum is that if the energy flux is to remain independent of radius, there must be a sharp jump in the ion pressure gradient so that ϵ_n jumps from a relatively large value to a small value. This corresponds to a pedestal in the ion pressure profile.

Finally, we comment briefly on the role of the development of sheared poloidal flows and particle transport in the regime where the η_i mode dominates the transport. Consistent with earlier simulations,[1] we find that the self-generated poloidal flows have a strong impact on the saturation of the turbulence in this regime. Elimination of the poloidal flows leads to a dramatic increase in the rates of transport. In a separate paper we discuss in more detail the mechanism for the generation of these flows.

The particle transport remains surprisingly large in the regime where the η_i driven turbulence dominates, the particle transport being on the order of 20%–30% of the ion energy transport. The electron heat transport is substantially smaller. The particle transport arises from the long parallel wavelength of the spectrum of turbulence. This long parallel wavelength component of the spectrum is a part of the structure of the linear eigenmode. The particle transport will also be discussed more fully in a separate publication.

[1] R. E. Waltz, G. D. Kerbel, and J. Milovich, Phys. Plasmas **1**, 2229 (1994).
[2] M. Kotschenreuther, W. Dorland, M. A. Beer, and G. W. Hammett, Phys. Plasmas **2**, 2381 (1995).
[3] P. N. Guzdar, J. F. Drake, D. C. McCarthy, A. B. Hassam, and C. S. Liu, Phys. Fluids B **5**, 3712 (1993).
[4] A. Zeiler, D. Biskamp, J. F. Drake, and P. N. Guzdar, Phys. Plasmas **3**, 2951 (1996).
[5] W. Horton, R. D. Estes, and D. Biskamp, Plasma Phys. **22**, 663 (1980).
[6] R. E. Waltz, Phys. Fluids **31**, 1962 (1988).
[7] S. Hamaguchi and W. Horton, Phys. Fluids B **2**, 1833 (1990).
[8] C. B. Kim, W. Horton, and S. Hamaguchi, Phys. Fluids B **5**, 1516 (1993).
[9] M. A. Beer and G. W. Hammett, Phys. Plasmas **3**, 4018 (1996).
[10] M. Kotschenreuther, W. Dorland, Q. P. Liu, G. W. Hammett, M. A. Beer, S. A. Smith, A. Bondeson, and S. C. Cowley, in *Fusion Energy 1996*, Proceedings of the 16th International Conference, Montreal (International Atomic Energy Agency, Vienna, 1997), Vol. 2, p. 371.
[11] J. F. Drake, A. Zeiler, and D. Biskamp, Phys. Rev. Lett. **75**, 4222 (1995).
[12] B. D. Scott, Plasma Phys. Controlled Fusion **39**, 471 (1997).
[13] B. D. Scott, Phys. Rev. Lett. **65**, 3289 (1990).
[14] S. V. Novakovskii, P. N. Guzdar, J. F. Drake, and C. S. Liu, Phys. Plasmas **2**, 781 (1995).
[15] G. W. Hammett, M. A. Beer, W. Dorland, S. C. Cowley, and S. A. Smith, Plasma Phys. Controlled Fusion **35**, 973 (1993).
[16] A. Zeiler, J. F. Drake, and B. Rogers, Phys. Plasmas **4**, 2134 (1997).
[17] H. Zohm, W. Suttrop, H. J. de Blank, R. J. Buttery, D. A. Gates, J. A. Heikkinen, W. Herrmann, A. Kallenbach, T. Kass, M. Kaufmann, T. Kurki-Sonio, B. Kurzan, M. Maraschek, H. Reimerdes, F. Ryter, H. Salzmann, J. Schweinzer, J. Stober, and the ASDEX Upgrade, ECRH, ICRH, and NBI teams, in Ref. 10, Vol. 1, p. 439.
[18] R. J. Groebner, T. S. Carlstrom, K. H. Burrell, S. Coda, E. J. Doyle, P. Gohil, K. W. Kim, R. Maingi, R. A. Moyer, Q. Peng, C. L. Rettig, T. L. Rhodes, D. P. Schissel, G. M. Staebler, R. D. Stambaugh, D. M. Thomas, and J. G. Watkins, in Ref. 10, Vol. 1, p. 867.
[19] A. E. Hubbard, J. A. Goetz, M. J. Greenwald, I. H. Hutchinson, Y. In, J. H. Irby, B. LaBombard, P. J. O'Shea, J. A. Snipes, P. C. Stek, Y. Takase, S. M. Wolfe, and the Alcator group, in Ref. 10, Vol. 1, p. 875.
[20] A. B. Hassam and R. M. Kulsrud, Phys. Fluids **22**, 2097 (1979).
[21] A. Zeiler, J. F. Drake, and D. Biskamp, Phys. Plasmas **4**, 991 (1997).
[22] M. Ottaviani, F. Romanelli, R. Benzi, M. Briscolini, P. Santangelo, and S. Succi, Phys. Fluids B **2**, 67 (1990).
[23] F. Romanelli, Phys. Fluids B **1**, 1018 (1989).
[24] A. Dimits, T. J. Williams, J. A. Byers, and B. I. Cohen, Phys. Rev. Lett. **77**, 71 (1996).
[25] The ASDEX team, Nucl. Fusion **29**, 1959 (1989).
[26] W. Suttrop, H. J. de Blank, G. Haas, H. Murmann, O. Gehre, H. Reimerdes, F. Ryter, H. Salzmann, J. Schweinzer, J. Stober, H. Zohm, ASDEX Upgrade team, NI team, and ICRH team, in *Proceedings of the 23rd European Physical Society Conference on Controlled Fusion and Plasma Physics*, Kiev (European Physical Society, Geneva, 1996), Vol. 1, p. 47.